Molecular Therapy
Nucleic Acids
Original Article

Base editing rescues acid α-glucosidase function in infantile-onset Pompe disease patient-derived cells

Chloe L. Christensen,[1] Shih-Hsin Kan,[1] Perla Andrade-Heckman,[1] Allisandra K. Rha,[1] Jerry F. Harb,[1] and Raymond Y. Wang[2,3]

[1]CHOC Children's Research Institute, Orange, CA 92868, USA; [2]Division of Metabolic Disorders, CHOC Children's Specialists, Orange, CA 92868, USA; [3]Department of Pediatrics, University of California, Irvine, School of Medicine, Irvine, CA 92697, USA

Infantile-onset Pompe disease (IOPD) results from pathogenic variants in the *GAA* gene, which encodes acid α-glucosidase. The correction of pathogenic variants through genome editing may be a valuable one-time therapy for PD and improve upon the current standard of care. We performed adenine base editing in human dermal fibroblasts harboring three transition nonsense variants, c.2227C>T (p.Q743*; IOPD-1), c.2560C>T (p.R854*; IOPD-2), and c.2608C>T (p.R870*; IOPD-3). Up to 96% adenine deamination of target variants was observed, with minimal editing across >50 off-target sites. Post-base editing, expressed GAA protein was up to 0.66-fold normal (unaffected fibroblasts), an improvement over affected fibroblasts wherein GAA was undetectable. GAA enzyme activity was between 81.91 ± 13.51 and 129.98 ± 9.33 units/mg protein at 28 days post-transfection, which falls within the normal range (50–200 units/mg protein). LAMP2 protein was significantly decreased in the most robustly edited cell line, IOPD-3, indicating reduced lysosomal burden. Taken together, the findings reported herein demonstrate that base editing results in efficacious adenine deamination, restoration of GAA expression and activity, and reduction in lysosomal burden in the most robustly edited cells. Future work will assess base editing outcomes and the impact on Pompe pathology in two mouse models, *Gaa*$^{c.2227C>T}$ and *Gaa*$^{c.2560C>T}$.

INTRODUCTION

Pompe disease (PD; OMIM: #232300) is an inherited metabolic disorder that presents primarily as skeletal and cardiac myopathy but also manifests neurologically.[1] Untreated patients with the most severe form, infantile-onset PD (IOPD), die in infancy from cardiorespiratory failure, respiratory muscle weakness, and hypertrophic cardiomyopathy. PD has been associated with more than 650 pathogenic variants in *GAA* (GenBank: NM_000152.5),[2,3] the gene that encodes acid α-glucosidase (GAA; E.C. 3.2.1.20)—a hydrolase required for lysosomal glycogen catabolism. Most pathogenic variants in *GAA* are specific to a single patient,[4] but some do occur more frequently. The most common pathogenic variant associated with IOPD is *GAA* c.2560C>T (p.R854*; global allele frequency = 0.00021) and has increased prevalence among African Americans (allele frequence = 0.00189).[5,6]

While enzyme replacement therapy (ERT) remains the standard of care, patients require life-long biweekly infusions where >95% eventually produce detectable antibodies to recombinant human (rh) GAA,[7] resulting in markedly reduced treatment efficacy.[8] Additionally, a low abundance of mannose-6-phosphate receptors on the surface of skeletal muscle cells prevents rhGAA from gaining entry to many muscles affected in patients with PD.[9,10] Unless treated with immunomodulation before the first exposure to rhGAA,[11] patients who are immunologically naive to GAA (cross-reactive immunologic material [CRIM] negative) develop far greater antibody titers than those who are CRIM positive.[12,13] In most cases, variants resulting in premature termination codons lead to nonsense-mediated decay of *GAA* transcripts that is associated with CRIM-negative status.[12]

Recent studies aim to evaluate the efficacy of next-generation receptor-targeting rhGAA[14] and pharmacological chaperone therapies,[15] but both strategies involve ongoing, indefinite administration. Investigations have also focused on liver-[16] and muscle-directed[17] gene therapies, yet the non-integrating nature of adeno-associated virus (AAV) means that the exogenous gene could be lost over time. The development of permanent and potentially single-dose therapeutic strategies for patients with PD is paramount.

Substantial recent expansion of, and improvement on, existing genome editing systems has allowed permanent and precise genomic modifications with high efficiency in mammalian cells[18–20] while simultaneously improving delivery mechanisms by reducing genome editor size to mitigate AAV cargo limits.[21–23] Further work has focused on the development of techniques to specifically control spatial[24] and temporal[25] cargo expression. Base editors, which

Received 21 November 2023; accepted 16 May 2024;
https://doi.org/10.1016/j.omtn.2024.102220.

Correspondence: Raymond Y. Wang, Division of Metabolic Disorders, CHOC Children's Specialists, Orange, CA 92868, USA.
E-mail: rawang@choc.org

A

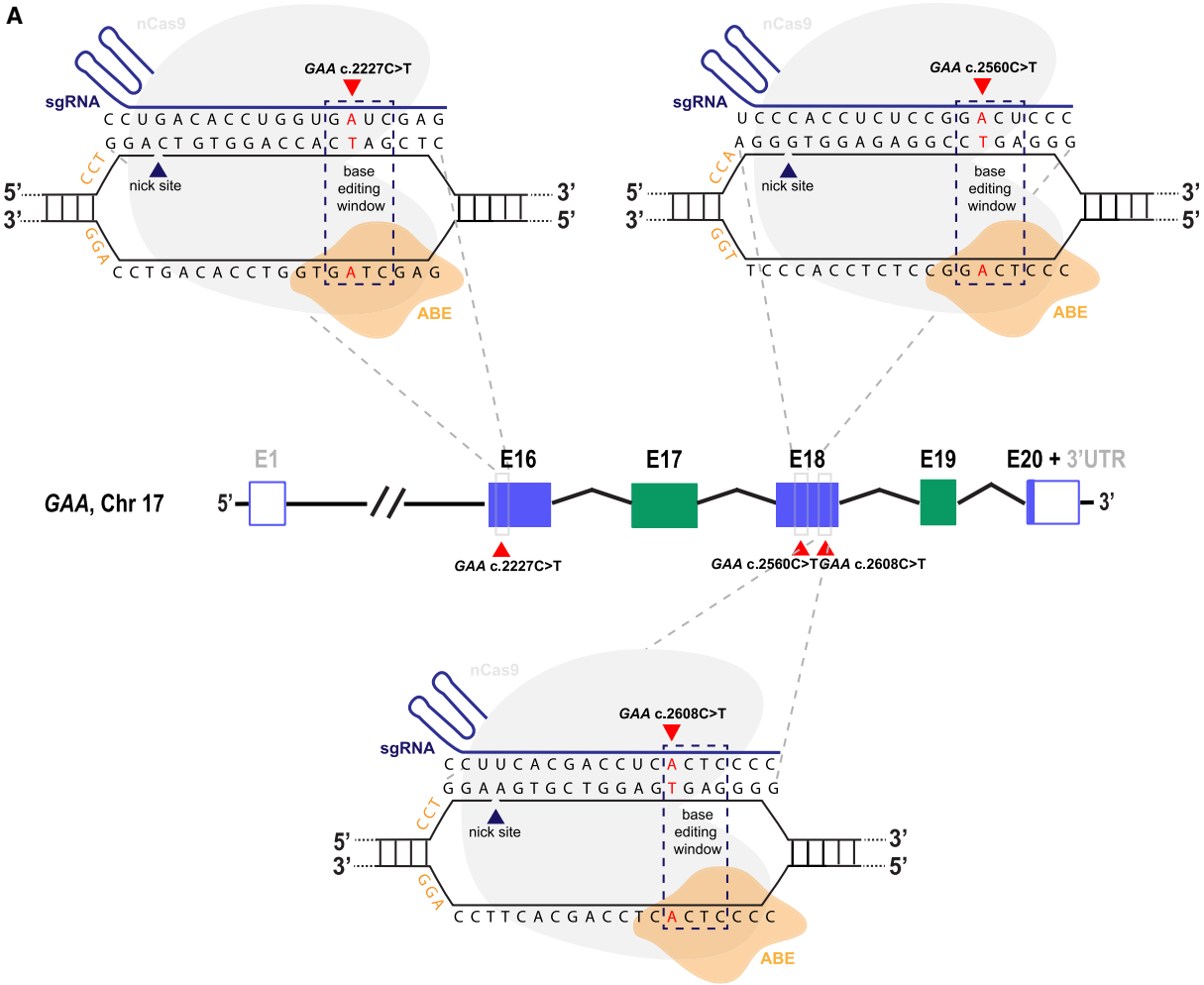

B

Cell Line	Target Variant	Exon	Protospacer sequence (5'→ 3')	Target Adenine Location	PAM
IOPD-1	c.2227C>T	16	GAG|CTAG|TGGTCCACAGTCC	A6	AGG
IOPD-2	c.2560C>T	18	CCC|TCAG|GCCTCTCCACCCT	A6	TGG
IOPD-3	c.2608C>T	18	CCC|CTCA|CTCCAGCACTTCC	A7	AGG

C

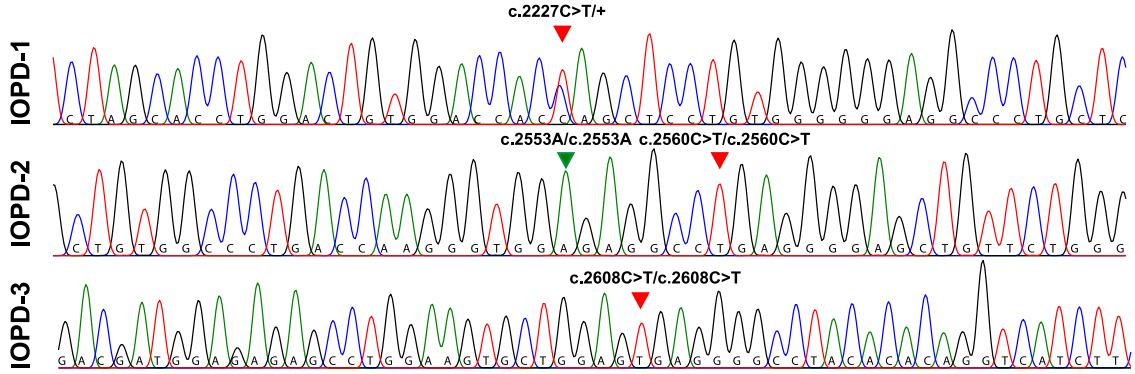

(legend on next page)

deaminate cytosine to thymine or adenine to guanine, are of particular interest for targeting pathogenic variants *in vivo* due to their high specificity and low probability of causing insertions/deletions (indels) at off-target sites.[19,26] Numerous studies have assessed base editing as a therapeutic strategy for monogenic disorders,[19,27,28] and base editing techniques have now progressed to clinical trials (ClinicalTrials.gov: NCT05398029, accessed February 10, 2023). Canonical base editing may be suitable for the correction of T>C, C>T, G>A, or A>G transition mutations in *GAA*, and the development of prime editors and next-generation base editors, capable of inducing transversions, further expands the repertoire of targetable PD variants.[29–31] Here, our aim was to use adenine base editing (ABE) to correct three pathogenic *GAA* transition variants (c.2227C>T, c.2560C>T, and c.2608C>T) in human dermal fibroblasts (HDFs) derived from patients with IOPD. ABE was found to efficiently correct all three variants, leading to the production of functional GAA enzyme, with minimal off-target editing. This study is the first demonstration of therapeutic genome editing in *GAA* and will serve as a foundation for the development of personalized base editing strategies for patients with PD and other monogenic disorders.

RESULTS

Three transition variants in *GAA* are amenable to ABE

We identified three *GAA* variants that are known to be pathogenic and are putative targets for ABE: c.2227C>T, c.2560C>T, and c.2608C>T. All three transition variants are situated proximally to an NGG PAM on the antisense strand, placing the target adenine within the activity window of canonical ABEs (Figures 1A and 1B).[26] Bystander adenines are not present within the activity windows at any of these three sites, reducing the likelihood of undesired adenine deamination near the sites of interest. We obtained HDFs from two patients. One patient harbors *GAA* c.2227C>T (p.Q743*) and c.258dupC (p.N87QfsX9) compound heterozygous pathogenic variants. This cell line will be hereafter referred to as IOPD-1. The second patient is homozygous for the *GAA* c.2608C>T (p.R870*) pathogenic variant and will be referred to as IOPD-3. We also obtained HDFs, homozygous for *GAA* c.2560C>T (p.R854*), from the Coriell Institute for Medical Research (GM00338); this cell line is denoted as IOPD-2. To confirm the expected genotype, all three cell lines were Sanger sequenced (Figure 1C). IOPD-2 was found to have a benign synonymous single-nucleotide variant (SNV), *GAA* c.2553G>A. The ancestral c.2553G has a minor allele frequency of 0.49062, and the current global allele frequency of c.2553A is 57% (gnomAD, accessed September 7, 2023). Of note, all four *GAA* c.2560C>T cell lines commercially available through the Coriell Institute of Medical Research harbor *GAA* c.2553A in homozygosity (GM00244, GM00248, GM00338, and GM20122; Figure S1).

All three cell lines showed appreciable levels of ABE, detectable upon Sanger sequencing at 4, 14, and 28 days post-nucleofection with variant-specific *GAA*-targeting single guide RNA (sgRNA) and ABEmax, when compared to mock conditions (Figures 2A and 2B). ABE efficiencies were as high as 100% ± 0%, 42% ± 13%, and 72% ± 4% for IOPD-1, -2, and -3, respectively, as measured via Sanger sequencing (Figure 2B). Complete editing of the variant-harboring allele in the IOPD-1 HDF line is particularly interesting. Given that this is a heterozygous cell line (50% of *GAA* alleles harbor c.2227C), this indicates that the target allele was fully edited to c.2227C across the HDF populations ($n = 8$). Furthermore, corrected alleles were detected in edited HDF populations 6–10 passages post-base editing, with no observed evidence of editing loss in any of the three cell lines (Figure S2). A secondary *in silico* assessment using EditR[32] showed similar editing efficiencies (Figure 2C). To explore these findings in further depth and to assess low-frequency protospacer-proximal adenine deamination and indels, targeted amplicon deep sequencing was performed 4 and 14 days post-nucleofection. Targeted amplicon deep sequencing with a coverage of >16,000×/sample showed similar average editing efficiencies across adenine-base-edited cell populations (95.61% ± 1.48%, 31.65% ± 1.13%, and 67.91% ± 1.97% at 14 days post-transfection for IOPD-1, -2, and -3, respectively); however, none of the IOPD-1 samples reached complete target adenine deamination, demonstrating the improved detection limit of next-generation sequencing over Sanger sequencing (Figure 2D).

Additionally, we detected minute levels of adenine deamination above baseline, outside of the canonical activity window, at protospacer positions A12–16. Indels were measured above baseline in IOPD-1 and -3 alleles with a frequency <1.50% ± 0.27% (Figure 2D). The greatest adenine deamination was measured 14 days post-transfection at IOPD-3-targeting protospacer position A12 with 0.75% ± 0.05% vs. 0.25% ± 0.01% in mock cells ($p = 0.0001$) (Figure 2D; Table S1). This bystander edit results in a missense mutation (p.L868P), which may impact the overall functional GAA produced; however, this variant, as well as any indels, would only impact a small proportion of total restored GAA given the low proportion of alleles with these unintended alterations. All adenine deamination across the target sites occurred at a frequency of <0.8% (Figure 2D; Table S1), which falls within sequencing and PCR error rates.[35]

Figure 1. Three pathogenic PD variants are targets for canonical ABE

(A) Schematic representation of adenine base editors interacting with protospacer sequences complementary to the region of three pathogenic IOPD variants, *GAA* c.2227C>T, c.2560C>T, and c.2608C>T (red) and their PAM sites (orange). (B) Tabulated protospacer sequences used for *GAA* c.2227T, c.2560T, and c.2608T base editing. Target adenines are at position six or seven (A6 or A7; 5′ protospacer nucleotide is position one). Canonical base editing activity windows are defined by $|n_4|$ and span protospacer position A4-7. (C) Sanger sequencing electropherograms of amplified genomic DNA derived from IOPD-1 to -3 cell lines. IOPD-1 harbors *GAA* c.2227C>T in compound heterozygosity with *GAA* c.258dupC (data not shown). IOPD-2 harbors *GAA* c.2560C>T in homozygosity. A benign synonymous variant exists within the protospacer region of the c.2560T-targeting single guide RNA (green arrow; ancestral G: MAF 0.49062). IOPD-3 harbors *GAA* c.2608C>T in homozygosity.

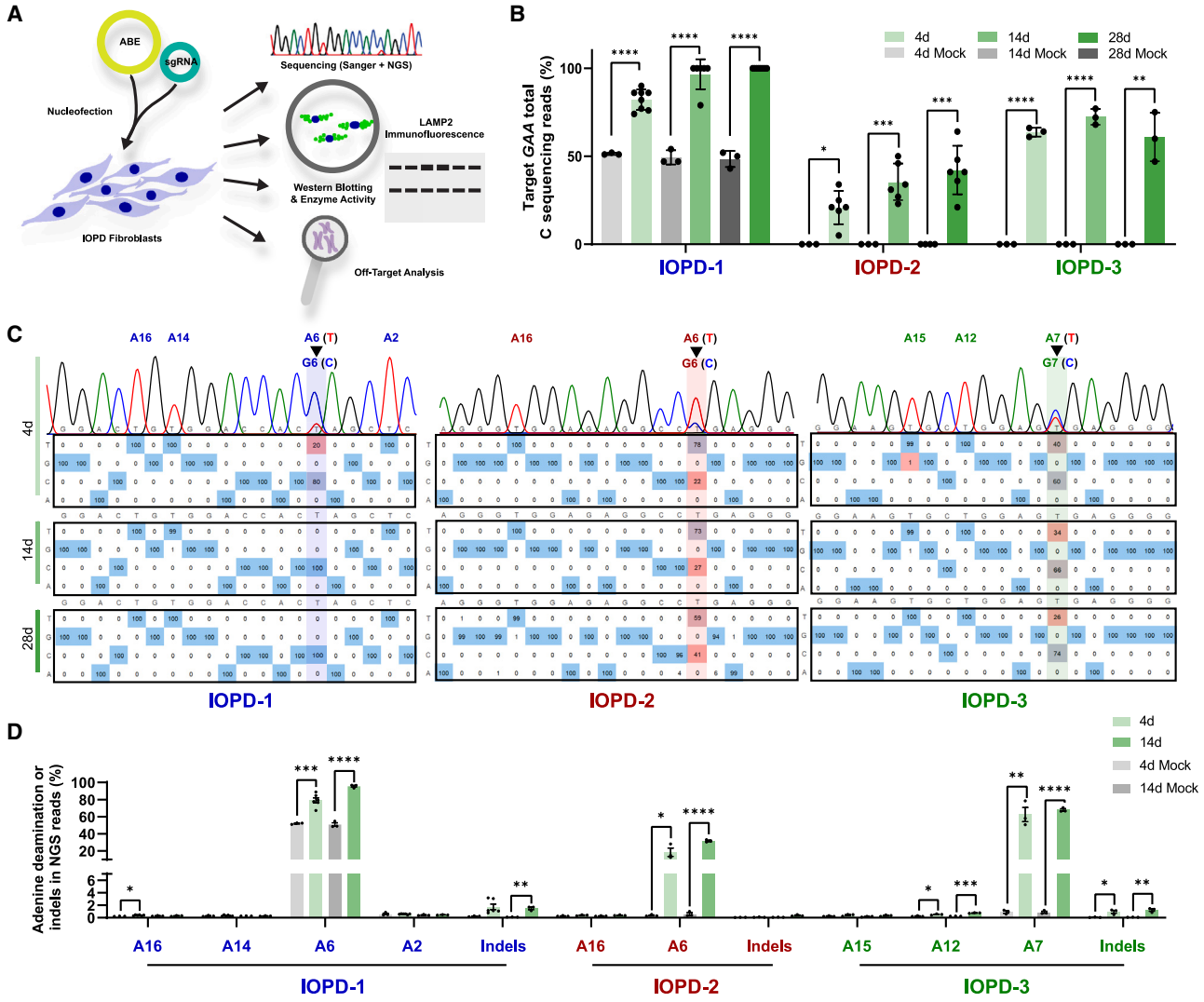

Figure 2. ABE results in significant target adenine conversion in dermal fibroblasts derived from patients with PD

(A) Schematic of ABE cargo delivery and subsequent efficacy and specificity assessments. (B) Percentage of Sanger sequencing reads revealing a C nucleotide at the target site 4, 14, and 28 days post-nucleofection in IOPD-1, -2, and -3 dermal fibroblast populations compared to mock cells. Electropherograms were assessed using the Synthego ICE analysis tool v.2.[33] Of note, the IOPD-1 cell line is compound heterozygous for *GAA* c.2227C>T/c.258dupC (exon 16, exon 2), and only one allele of exon 16 was targeted for ABE. Therefore, 50% of the target "C" comes from the unaffected allele. (C) Nucleotide plots representing adenine deamination across the protospacer-spanning regions at 4, 14, and 28 days post-nucleofection in IOPD-1, -2, and -3 HDF populations. A-to-G conversion (antisense strand) is evidenced by C nucleotide base calls within nucleotide plots. The target adenine sites are highlighted in blue, red, and green for IOPD-1, -2, and -3, respectively. Electropherograms were assessed using EditR 1.0.10.[32] (D) Targeted amplicon deep sequencing of protospacer-spanning regions at 4 and 14 days post-nucleofection in IOPD-1, -2, and -3 HDF populations (>16,000× coverage/data point) compared to mock cells. Next-generation sequencing (NGS) data were assessed using CRISPResso2.[34] Two-tailed unpaired Student's t tests; *$p < 0.05$, **$p < 0.01$, ***$p < 0.001$, and ****$p < 0.0001$. All error bars show mean ± standard deviation.

Since *GAA* c.2553G has a high global allele frequency, we designed a protospacer harboring a mismatched cytosine complementary to this SNV. If this mismatch is tolerable, resulting in appreciable editing efficiencies in cell lines harboring the c.2553G>A variant, then this would allow for a universal sgRNA independent of SNV genotype. Transfection of HDFs with plasmids expressing c.2553G-harboring sgRNA and ABE did not yield detectable base editing in IOPD-2 HDFs (Figure S3), indicating that nucleotide mismatch at protospacer position A12 in this sgRNA is not tolerated.

Adenine-base-edited fibroblasts express enzymatically active GAA

Populations of cells treated with ABE exhibited restoration of GAA enzyme activity, achieving levels that are within the expected normal range for unaffected HDFs (45–180 units/mg protein) for all three

genotypes at 28 days post-transfection (Figure 3A).[2] Enzyme activity rates were measured as 118.46 ± 7.12 ($p < 0.0001$), 81.91 ± 13.51 ($p = 0.0011$), and 129.98 ± 9.33 units/mg protein ($p < 0.0001$) for IOPD-1, -2, and -3, respectively, at 28 days post-transfection (Figure 3A), and GAA enzyme activity was maintained within the normal range long term (6–12 passages post-base editing; Figure S2). Western blots confirm the presence of GAA protein after ABE (Figure 3B). The total GAA protein amounts detected post-editing were determined to be 0.52-, 0.31-, and 0.66-fold normal (unaffected HDFs) for IOPD-1, -2, and -3, respectively, when normalized to the loading control, GAPDH. GAA protein was not detected in untreated IOPD HDFs, confirming the CRIM-negative status associated with all three genotypes. Digestion of GAA with endoglycosidase H (Endo H) reveals that GAA-produced post-base editing has the same pattern of Endo H sensitivity and resistance as wild-type GAA, providing evidence for the normal trafficking and glycosylation of GAA in base-edited cells (Figure S4).[36]

Assessment of LAMP2 through immunofluorescence shows bright punctate signal in IOPD dermal fibroblasts (Figure 3C). Quantification of LAMP2 immunofluorescence shows significant increases in LAMP2 signal intensity between unaffected and affected dermal fibroblasts for IOPD-2, but not IOPD-1, and shows a decrease between unaffected and affected dermal fibroblasts for IOPD-3 and is therefore inconclusive (Figure S5). Total LAMP2 protein quantified via western blotting post-base editing is not significantly reduced in IOPD-1 (1.21- vs. 0.91-fold) or IOPD-2 (1.87- vs. 1.97-fold) dermal fibroblasts, but normalization ($p = 0.9796$) is measured post-base editing in IOPD-3 fibroblasts (2.20- vs. 1.06-fold) (Figure 3B). Observable differences in periodic acid-Schiff (PAS)-positive polysaccharide inclusions were not detected across unaffected, affected, and ABE-treated HDFs (Figure S6).

Adenine-base-edited dermal fibroblasts have minimal off-target edits

To assess ABE-induced indels or adenine deamination, 52 off-target sites identified *in vitro* by CIRCLE-seq or nominated by Cas-OFFinder and Hsu off-target scores were analyzed (Figures 4 and S7).[36–38] Deep sequencing of these sites with >1,000× coverage demonstrated minimal off-target editing. OT18 (IOPD-3; intron 5 of *ZNF536*) and OT8 (IOPD-3; intron 5 of *NCOR2*) were found to have significant adenine deamination (A7: 7.98% ± 1.49% vs. 0.62% ± 0.02%, $p = 0.001$, and A15: 0.80% ± 0.22% vs. 0.35% ± 0.12% $p = 0.0362$; 0.85% ± 0.14% vs. 0.59% ± 0.05%, $p = 0.0421$) after treatment with IOPD-3-targeting sgRNA and ABE (Figure 4). Adenine deamination at these off-target sites is expected to neither result in disruption of a 5′ or 3′ splice site nor eliminate a branch-point site and is therefore not predicted to impact gene expression.[39,40] An arbitrary threshold of adenine deamination or indels of 0.8% was applied to account for sequencing and PCR error rates.[35] All other sequenced sites did not show adenine deamination or indels above background. Specific adenine deamination and indel percentages and p values are shown in Tables S2 and S3.

DISCUSSION

We herein report the first base editing of genetic variants causative for PD. In this study, we demonstrate efficient ABE of three IOPD variants (c.2227C>T, c.2560C>T, and c.2608C>T) in HDFs, achieving up to 96% editing of the c.2227C>T variant in the IOPD-1 heterozygous cell line and 67% editing in a c.2608C>T homozygous cell line (IOPD-3). Target variant base editing led to restoration of enzyme activity, measured as 118.46 ± 7.12 ($p < 0.0001$), 81.91 ± 13.51 ($p = 0.0011$), and 129.98 ± 9.33 ($p < 0.0001$) units/mg protein for IOPD-1, -2, and -3, respectively, at 28 days post-transfection, rates comparable to what is measured in unaffected HDFs. Normalization of LAMP2 was observed in the most robustly edited cell line (IOPD-3), indicating a reduction in lysosomal burden.

We chose these three variants due to their presence in accessible patient-derived cells, their targetability by ABEs, and, in the case of c.2560C>T, the frequency of this variant in the IOPD patient population. Although c.2227C>T has been reported only once, c.2560C>T and c.2608C>T have 77 and 10 associated patients, respectively, reported in the PD *GAA* variant database as of 2021.[2] Given that there are hundreds of variants known to cause IOPD and that patient-specific SNVs within the protospacer-targeting region can hinder editing efficiency (Figure S3), designing and assessing personalized genome editing strategies may prove challenging. Alternative variant-indiscriminate strategies that employ next-generation genome editing approaches, such as twin prime editing,[18] should also be explored to encompass the wide range of PD-causing *GAA* variants.

Interestingly, we observed increased editing efficiency over time. Given that the half-life of plasmid DNA in mammalian cells is approximately 20 h, and plasmid DNA has been found to persist for at least 6 days post-transfection, target alleles may undergo editing beyond the initial 4 day time point.[41] This finding may also be indicative of a selective advantage for cells expressing functional GAA enzyme *in vitro*, but further investigation is necessary to determine the mechanism underlying the observed increases in overall editing efficiency and GAA enzyme activity over time. Additionally, even though considerable base editing is measured by deep sequencing at 4 days post-transfection, GAA activity is ≤25% of normal rates (Figures 2D and 3A). Rates of GAA activity that fall within the normal range are later observed at 14 (IOPD-1 and -3) or 28 days (IOPD-2) and are maintained within this normal range long term (6–12 passages post-base editing; Figures 3A and S2).

GAA protein expression post-base editing was measured as 0.52-, 0.31-, and 0.66-fold normal (unaffected HDFs) for IOPD-1, -2, and -3, respectively, correlating with editing efficiencies (Figure 3B). To evaluate the intracellular location of GAA post-base editing, we digested GAA with Endo H, a specific endoglycosidase that cleaves mannose-rich oligosaccharides and is used to monitor intracellular trafficking indirectly.[42,43] This assay revealed the same pattern of Endo H-sensitive and -resistant banding for GAA derived from unaffected and ABE-treated IOPD-1 fibroblasts, providing evidence of

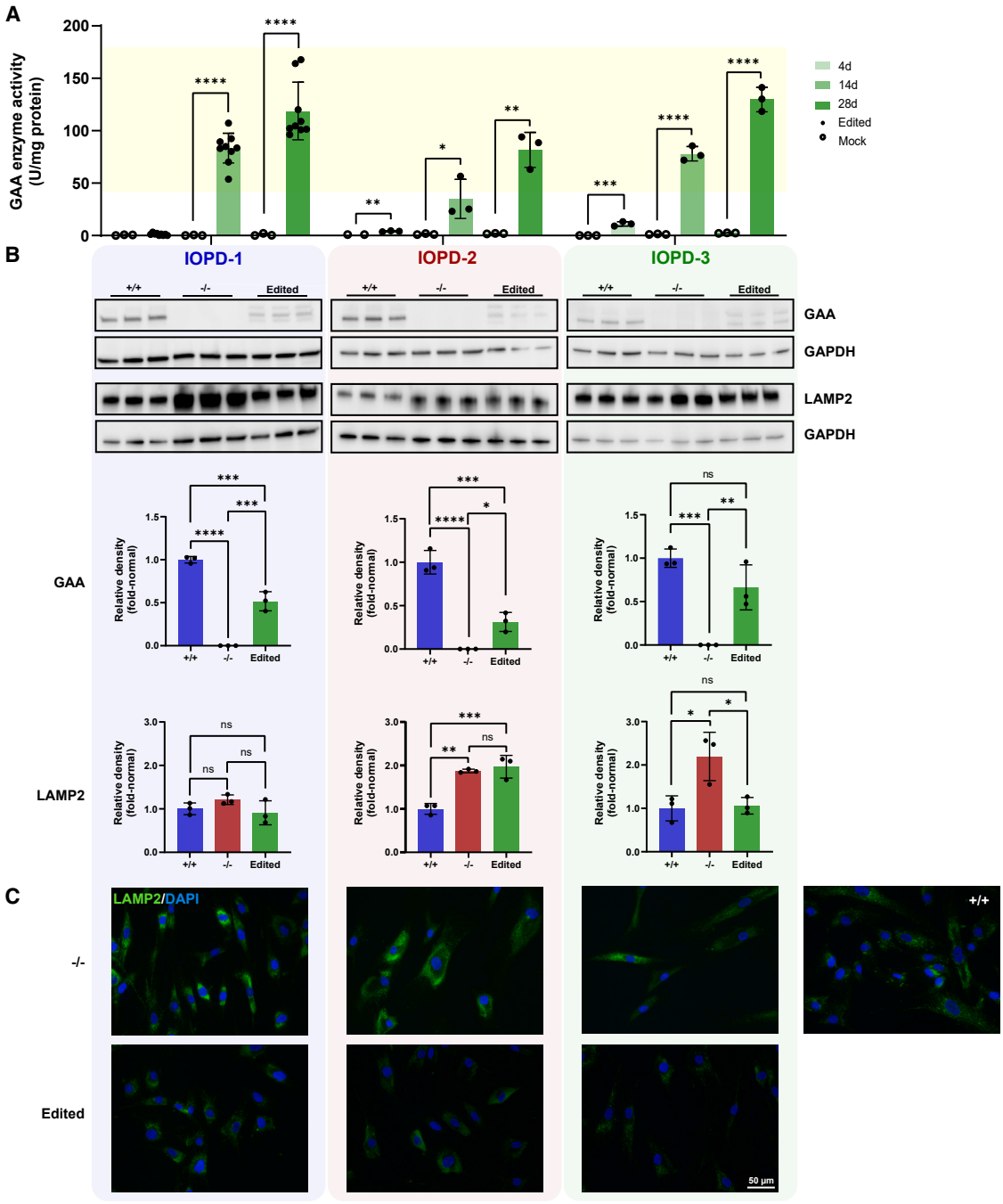

Figure 3. Edited human dermal fibroblasts have restored GAA enzyme activity and reduced LAMP2

(A) GAA enzyme activity at 4, 14, and 28 days post-nucleofection in IOPD-1, -2, and -3 dermal fibroblast populations compared to mock cells. Comparisons were analyzed using two-tailed unpaired Student's t tests; *$p < 0.05$, **$p < 0.01$, ***$p < 0.001$, and ****$p < 0.0001$. Yellow shading represents the normal range of GAA activity in cultured unaffected HDFs (45–180 units/mg protein).[2] (B) Western blots of IOPD-1, -2, and -3 (−/−), ABE-treated IOPD-1, -2, and -3 (edited), and unaffected (+/+) HDFs using antibodies to detect GAA, LAMP2, and GAPDH. Quantification of western blots for LAMP2 and GAA normalized to GAPDH and expressed as relative density (fold normal). Comparisons were analyzed using one-way ANOVA with Tukey post-hoc test; *$p < 0.05$, **$p < 0.01$, ***$p < 0.001$, ****$p < 0.0001$, and ns, not significant. (C) Immunofluorescence photomicrographs showing LAMP2 signal (green) in IOPD-1, -2, and -3 (−/−), ABE-treated IOPD-1, -2, and -3 (edited), and unaffected (+/+) HDFs. Scale bar represents 50 µm. All error bars show mean ± standard deviation.

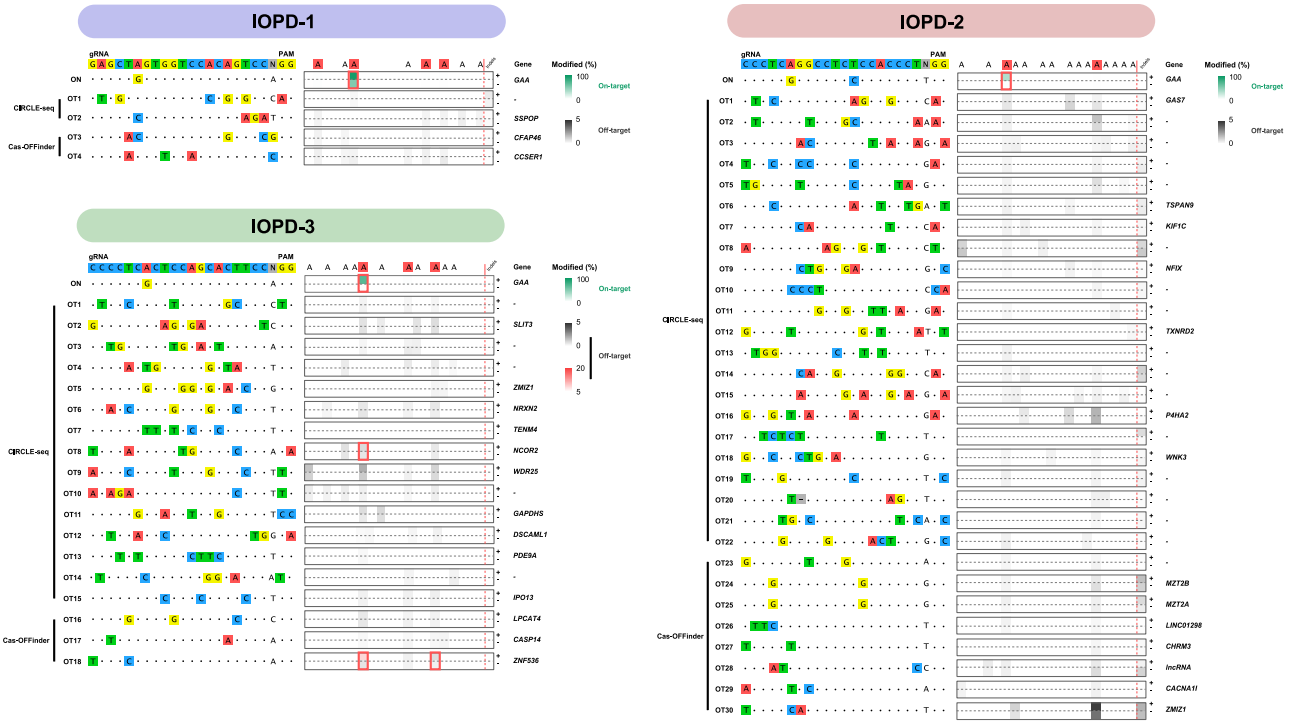

Figure 4. Targeted amplicon deep sequencing shows minimal off-target editing across *in-silico*- and *in-vitro*-predicted sites

Putative off-target sites were identified by *in vitro* CIRCLE-seq assay.[38] Further off-target sites were predicted *in silico* using Cas-OFFinder[36] allowing for up to three mismatches between protospacer and genomic site and cross-referenced to Hsu off-target scores.[37] In addition to CIRCLE-seq-identified off-target sites, Cas-OFFinder-predicted off-target sites with a Hsu off-target score >1 mapping to genomic coding or regulatory regions were PCR amplified for targeted amplicon deep sequencing. Resulting sequencing reads (>1,000× coverage/data point) from $n = 3$ independently nucleofected IOPD-1, -2, and -3 HDF populations for both ABE-treated (+) and mock (–) conditions were assessed using CRISPResso2.[34] Nucleotide percentages of modification at adenine sites present across the protospacer-spanning regions (shown above the plots) are represented as heatmaps (0%–5% modification shown in gray; 5%–20% modification shown in red). Indels are reported on the far right. Significant differences in nucleotide modification between ABE-treated and mock conditions as identified by two-tailed unpaired Student's t tests are represented by red boxes.

normal glycosylation and intracellular localization of GAA (Figure S4). The work of others has shown that, with ERT, rhGAA becomes trapped in the endocytic pathway and/or is mis-trafficked due to the existing autophagic impairments within murine muscle fibers.[44,45] Future studies are imperative to further interrogate the intracellular location of GAA post-base editing. In a recent study, co-therapy of ERT with 1,3-butanediol, a ketone precursor, and an antioxidant cocktail led to the greater attenuation of muscle pathology in *Gaa* knockout mice than ERT alone.[46] If cellular impairments are found to exist post-base editing, then co-treatment with similar compounds may also contribute to a reduction in PD pathology by mitigating autophagic dysfunction and will be explored in murine models of IOPD ($Gaa^{c.2227C>T}$ and $Gaa^{c.2560C>T}$).

Although we show that GAA produced in ABE-treated HDFs is effective at catabolizing an artificial substrate, we do not report biochemical measurements of the natural substrate, glycogen. Although skeletal and cardiac muscle accumulate glycogen in PD, which is rescued after ERT,[14] we found glycogen measurements to be inconclusive and unreproducible in fibroblasts. We performed PAS staining in HDFs with or without ABE treatment, as well as in an unaffected HDF cell line, and did not observe differences in PAS-positive polysaccharide inclusions across the cell lines or treatment conditions, providing further evidence that fibroblasts do not store appreciable amounts of glycogen (Figure S6). Glycogen levels were not assessed under glucose starvation or a regulated nutrient replenishment schedule, which, in addition to fibroblasts not being a primary store for glycogen, may contribute to challenges in reliably and reproducibly detecting glycogen. Furthermore, despite GAA enzyme activity measured within the normal range for all three ABE-treated cell lines, we observed a reduction in LAMP2 expression only in IOPD-3, the most efficiently edited cells. Future assessments of glycogen and LAMP2 levels in induced pluripotent stem cell-derived cardiomyocytes and murine myocytes post-ABE will be informative.

Finally, the impact of off-target editing was explored using both *in silico* (Cas-OFFinder and Hsu off-target scores) and *in vitro* (CIRCLE-seq) analyses, followed by targeted amplicon deep sequencing to identify bona fide off-target sites (Figure 4). Although more than 50 sites were assessed, only two sites, both in ABE-treated IOPD-3 cells, were found to have significant adenine deamination across the protospacer-targeting region. The impact on gene expression or function

is not expected, since adenine deamination is intronic at these sites and does not span predicted splice or branchpoint sites at either off-target site.

In conclusion, this study demonstrates efficient ABE of IOPD-causing variants *in vitro*, leading to the production of functional GAA and, in the most robustly edited cells, evidence of reduced lysosomal burden. Assessing the efficacy of and optimal delivery methods for genome editing-based therapeutics in murine models of IOPD is necessary. Immunogenicity to GAA is an expected hurdle for *in vivo* translation given that substantial antibody titers are produced in CRIM-negative patients in response to ERT.[7] The existence of split-intein ABEs[47] qualifies myotropic AAVs, such as AAVMYO[48] or MyoAAV,[49] as delivery approaches that may reduce possible immunogenicity to AAV, GAA, and ABE. Given these myotropic vectors specifically and effectively transduce skeletal muscle at far lower doses than AAV9, enhanced *GAA* correction in muscle with minimal off-target consequences in other tissues may be achieved. Additionally, temporal control of ABE expression through small-molecule drug-controlled switch elements[25] could further limit immunogenicity to editing machinery. Given that current therapeutic options for patients with IOPD are limited, the translation of these ABE strategies to patients may offer an efficacious, long-term therapy, and their safety and feasibility will be explored going forward. Future work will focus on the optimization of cassettes expressing ABE and sgRNA under a muscle-specific promoter, with a focus on temporal expression of ABE for minimal toxicity in mouse models harboring the variants targeted in this study ($Gaa^{c.2227C>T}$ and $Gaa^{c.2560C>T}$).

MATERIALS AND METHODS

Mammalian cell culture and genotyping

IOPD-1 and IOPD-3 primary HDFs were obtained via sterile skin punch biopsy following the provision of assent/informed consent (ethics approval: Children's Hospital of Orange County Institutional Review Board, #130990). IOPD-2 primary HDFs were acquired from the NIGMS Human Genetic Cell Repository at the Coriell Institute for Medical Research (GM00338). HDFs were cultured in Dulbecco's modified Eagle medium (Cytiva) supplemented with 15% (v/v) fetal bovine serum (Omega Scientific), 1% (v/v) MEM Non-Essential Amino Acids (Gibco), and either 1% (v/v) Antibiotic-Antimycotic (Gibco) or 37.5 μg/mL Primocin (Invivogen). Cells were maintained at 37°C with 5% CO_2. For genotyping, genomic DNA was PCR amplified using exon-specific primers (Table S4). Amplicons were purified using the Zymoclean Gel DNA Recovery Kit (Zymo Research) and Sanger sequenced (Eurofins Genomics).

DNA cloning and bacterial culture

Single-stranded DNA oligonucleotides were synthesized by Integrated DNA Technologies. Complementary spacers with *Bsm*BI-compatible overhangs were annealed and ligated to *Bsm*BI-digested BPK1520 plasmid, as described previously.[50] Where necessary, a 5′ G was added to the spacer sequence to promote transcriptional initiation under the U6 promoter. BPK1520 was a gift from Keith Joung (Addgene plasmid #65777; http://n2t.net/addgene:65777; RRID:Addgene_65777).[50] NEB 5-alpha Competent *E. coli* (High Efficiency; New England Biolabs) were transformed with ligated plasmids using standard protocols. pCMV_ABEmax_P2A_GFP was a gift from David Liu (Addgene plasmid #112101; http://n2t/addgene:112101; RRID:Addgene_112101).[19] Plasmids were purified using the ZymoPURE II Plasmid Midiprep Kit as per the manufacturer's protocol (Zymo Research). Oligonucleotide sequences are listed in Table S5.

In vitro ABE

HDFs were nucleofected with either 250 ng *GAA*-targeting sgRNA expression plasmid or 250 ng mock sgRNA expression plasmid (BPK1520) and 750 ng ABEmax expression plasmid using the 4D-Nucleofector X Unit (Lonza) and P2 Primary Cell 4D-Nucleofector X Kit (Lonza), as per the manufacturer's protocol, using program CA-137. Transfected cells ($0.5–2.0 \times 10^4$) were pelleted at 4, 14, and 28 days post-transfection. Cell pellets were lysed in preparation for enzyme activity assay using CelLytic M cell lysis reagent (Millipore Sigma) and for PCR and CIRCLE-seq using QuickExtract DNA Extraction Solution (LGC Biosearch Technologies) according to the manufacturer's protocols. Primers used for genomic DNA amplification are listed in Table S4. Sanger sequencing was performed by Eurofins Genomics. Base editing efficiency was assessed using Synthego ICE analysis tool v.2.[33] Output knockin scores were used to calculate the proportion of cytosine at the target variant site within the cell population. EditR v.1.0.10[32] was used to generate base editing table plots, where colored tiles indicate significance ($p < 0.01$). ab1 files were used as input for both analyses. All transfections were conducted in triplicate.

Target amplicon deep sequencing

Genomic DNA was amplified using PCR primers flanking the target region resulting in <250 bp DNA amplicons (Table S4). Amplicons were library prepped using the NEBNext Ultra II DNA Library Prep kit (New England Biolabs) according to the manufacturer's protocol, with the following modifications: DNA amplicons were 5′ phosphorylated using 10 U of T4 polynucleotide kinase (New England Biolabs) and in the presence of 1 mM ATP (New England Biolabs) at 37°C for 30 min and inactivated at 65°C for 20 min. Size selection of adaptor-ligated DNA was performed using AMPure XP Beads (Beckman Coulter) using a bead/sample ratio of 0.7×. Adaptor-ligated DNA was enriched using NEBNext Multiplex Oligos for Illumina (New England Biolabs), as per the manufacturer's protocol, with five PCR cycles. Average fragment sizes were quantified using an Agilent High Sensitivity DNA Chip on an Agilent 2200 TapeStation, and library concentration was quantified using the Qubit 1× dsDNA High Sensitivity Assay Kit (Invitrogen) on a Qubit 3 Fluorometer (Invitrogen). Pooled libraries were quantified using the Kapa Library Quantification Kit (Roche) and were run paired-end on a MiSeq (Illumina) using the MiSeq v.2 Nano 500 cycle Reagent Kit (Illumina). The MiSeq was controlled by Illumina MCS 1.6.2.1 software, and real-time data were conducted using Illumina RTA 1.18.54 software. Adenine deamination and indels were quantified using CRISPResso2 v.2.2.12[34] by aligning deep sequencing reads to a

reference sequence and were analyzed using base editing mode with "amplicon_min_alignment_score = 50" and all other parameters set to default.

GAA enzyme activity assay

Cell lysate was mixed with freshly prepared 6 mM 4-methylumbelliferyl-α-D-glucopyranoside substrate (Millipore Sigma) in McIlvaine citrate/phosphate buffer (pH 4.3) at a 1:1 ratio in a 96-well plate and incubated for 1 h at 37°C. Reactions were quenched with nine parts glycine carbonate buffer (pH 10.5), and fluorescence measurements were obtained using an Infinite M Plex spectrofluorophotometer (Tecan) at excitation and emission wavelengths of 360 and 450 nm, respectively. One activity unit was defined as 1 nmol 4-methylumbelliferone released per hour. Protein concentration was estimated using Pierce BCA Protein Assay Kit (Thermo Fisher Scientific), and bovine serum albumin provided from the kit was used as a standard. Measurements were made in triplicate and reported as specific activity (units of activity/mg of protein).

Western blot analysis

Western blotting was performed as previously described with 19 μg of total protein/sample.[51] Primary antibodies are as follows: LAMP2 mouse monoclonal antibody (1:1,500, Developmental Studies Hybridoma Bank [DSHB], RRID:AB_528129), GAA rabbit monoclonal antibody (1:500, R&D Systems, RRID:AB_2942097), and GAPDH rabbit polyclonal antibody (1:1,500, Novus Biologicals, RRID:AB_10002458). The LAMP2 antibody was deposited to the DSHB by August, J.T./Hildreth, J.E.K. (DSHB Hybridoma Product H4B4). Goat anti-mouse IgG-HRP conjugate antibody (1:3,000, Bio-Rad, RRID:AB_11125547) and goat anti-rabbit IgG-HRP conjugate antibody (1:3,000, Bio-Rad, RRID:AB_11125142) were used where applicable. Blots were quantified using ImageJ software,[52] and LAMP2 pixel densities were corrected to GAPDH and normalized to unaffected HDFs.

LAMP2 immunocytochemistry

Cells were fixed in 4% (v/v) Zinc Sulfate Formalin Fixative (EKI Industries), permeabilized in 1% (w/v) Saponin (Sigma-Aldrich), and blocked in 3% BSA (v/v; Gibco). Cells were incubated with LAMP2 mouse monoclonal primary antibody (1:200, DSHB, RRID:AB_528129) overnight at 4°C. Cells were incubated with donkey anti-mouse IgG-Alexa Fluor 488 conjugate antibody (1:1000, Molecular Probes, RRID:AB_141607) for 1 h at room temperature and mounted in VECTASHIELD Antifade Mounting Medium with DAPI (Vector Laboratories). Images were captured on a Keyence BZ-X800 imaging system at 40× magnification.

In silico off-target analysis

In silico prediction of putative off-target sites was performed using Cas-OFFinder[36] with an allowable mismatch ≤3, DNA and RNA bulge ≤0, and a 5′-NGG-3′ PAM. Predicted off-target sites were cross-referenced to off-target specificity scores generated in Benchling (Biology Software, 2023). Off-target sites identified with Cas-OFFinder that had a specificity score >1 and were located at protein-coding or regulatory sites were amplified for targeted amplicon deep sequencing.[37] Additional off-target sites of interest were also assessed (Figure S7).

CIRCLE-seq sample preparation and analysis

A minimum of 1 μg of genomic DNA/sample was sheared to an average size of 300 bp using the NEBNext Ultra II FS Enzyme Mix (New England Biolabs) as per the manufacturer's protocol. Sheared DNA was circularized and treated with SpCas9-sgRNA ribonucleoprotein complexes as previously described.[38] sgRNAs were synthesized by Synthego. The resulting linearized DNA was library prepped as described above but with 22 PCR cycles. Libraries were deep sequenced as described above. The resulting fastq files were merged, aligned to the hg19 reference assembly (http://www.broadinstitute.org/ftp/pub/seq/references/Homo_sapiens_assembly19.fasta), and compared to control reads using the CIRCLE-seq v.1.1 analysis pipeline (https://github.com/tsailabSJ/circleseq) with default manifest file parameters. Off-target sites identified using this method were assessed in ABE-treated and mock cell samples in triplicate using targeted amplicon deep sequencing and CRISPResso2[34] as described above.

Software and statistical analysis

Figures were prepared using Adobe Illustrator 27.7. Statistical analysis was performed on DNA, enzyme, and western blot quantifications in GraphPad Prism 10.0.1 (218) using Student's two-tailed unpaired t tests or one-way ANOVA with Tukey's post-hoc analysis. All data are expressed as mean ± standard deviation. All mean percentages of adenine deamination or indels at off-target sites that were <0.8% adenine deamination were excluded to account for sequencing and PCR error rates.[35]

DATA AND CODE AVAILABILITY

The data supporting the findings of this study are available from the corresponding authors upon reasonable request.

SUPPLEMENTAL INFORMATION

Supplemental information can be found online at https://doi.org/10.1016/j.omtn.2024.102220.

ACKNOWLEDGMENTS

This work was supported by the Campbell Foundation of Caring, the CHOC Foundation (One Wish, 2019), the Larry and Helen Hoag Foundation, and the National Institutes of Health (R01AR079223, 2021). We are extremely grateful to the families of children with PD who participated in this study. We also thank the University of California, Irvine, Genomics Research and Technology Hub for their next-generation sequencing services and The Genomics Research and Technology Hub (formerly the Genomics High-Throughput Facility) Shared Resource of the Cancer Center Support Grant (P30CA-062203); the Single Cell Analysis Core shared resource of Complexity, Cooperation and Community in Cancer (U54CA217378); the Genomics-Bioinformatics Core of the Skin Biology Resource Based Center @ UCI (P30AR075047) at the University of California, Irvine;

and National Institutes of Health shared instrumentation grants 1S10RR025496-01, 1S10OD010794-01, and 1S10OD021718-01. The LAMP2 monoclonal antibody developed by Johns Hopkins University School of Medicine was obtained from the DSHB, created by the Eunice Kennedy Shriver National Institue of Child Health and Human Development of the National Institutes of Health, and maintained at The University of Iowa, Department of Biology (Iowa City, IA 52242, USA). Much gratitude goes to the CHOC Research Computational and Data Sciences team, with a special thanks to Dr. Peyman Kassani. We are also grateful to Max Chen for assistance with data entry.

AUTHOR CONTRIBUTIONS

C.L.C. conceived the study and led the experimental design. S.-H.K., A.K.R., J.F.H., and R.Y.W. contributed to the experimental design. C.L.C., S.-H.K., P.A.-H., and A.K.R. performed experiments and data collection. C.L.C. and S.-H.K. performed data analysis. C.L.C., A.K.R., S.-H.K., and R.Y.W. interpreted the data. C.L.C. wrote the manuscript with contributions from the co-authors. R.Y.W. supervised and obtained funding for the study.

DECLARATION OF INTERESTS

The authors declare no competing interests.

REFERENCES

1. Korlimarla, A., Lim, J.-A., Kishnani, P.S., and Sun, B. (2019). An emerging phenotype of central nervous system involvement in Pompe disease: from bench to bedside and beyond. Ann. Transl. Med. *7*, 289. https://doi.org/10.21037/atm.2019.04.49.

2. de Faria, D.O.S., In 't Groen, S.L.M., Hoogeveen-Westerveld, M., Niño, M.Y., van der Ploeg, A.T., Bergsma, A.J., and Pijnappel, W.W.M.P. (2021). Update of the Pompe variant database for the prediction of clinical phenotypes: Novel disease-associated variants, common sequence variants, and results from newborn screening. Hum. Mutat. *42*, 119–134. https://doi.org/10.1002/humu.24148.

3. Hernández-Arévalo, P., Santotoribio, J.D., Delarosa-Rodríguez, R., González-Meneses, A., García-Morillo, S., Jiménez-Arriscado, P., Guerrero, J.M., and Macher, H.C. (2021). Genotype–phenotype correlation of 17 cases of Pompe disease in Spanish patients and identification of 4 novel GAA variants. Orphanet J. Rare Dis. *16*, 233. https://doi.org/10.1186/s13023-021-01864-8.

4. Peruzzo, P., Pavan, E., and Dardis, A. (2019). Molecular genetics of Pompe disease: a comprehensive overview. Ann. Transl. Med. *7*, 278. https://doi.org/10.21037/atm.2019.04.13.

5. Kishnani, P.S., Gibson, J.B., Gambello, M.J., Hillman, R., Stockton, D.W., Kronn, D., Leslie, N.D., Pena, L.D.M., Tanpaiboon, P., Day, J.W., et al. (2019). Clinical characteristics and genotypes in the ADVANCE baseline data set, a comprehensive cohort of US children and adolescents with Pompe disease. Genet. Med. *21*, 2543–2551. https://doi.org/10.1038/s41436.

6. Park, K.S. (2021). Carrier frequency and predicted genetic prevalence of Pompe disease based on a general population database. Mol. Genet. Metab. Rep. *27*, 100734. https://doi.org/10.1016/j.ymgmr.2021.100734.

7. Kishnani, P.S., Goldenberg, P.C., DeArmey, S.L., Heller, J., Benjamin, D., Young, S., Bali, D., Smith, S.A., Li, J.S., Mandel, H., et al. (2010). Cross-reactive immunologic material status affects treatment outcomes in Pompe disease infants. Mol. Genet. Metab. *99*, 26–33. https://doi.org/10.1016/j.ymgme.2009.08.003.

8. van Gelder, C.M., Hoogeveen-Westerveld, M., Kroos, M.A., Plug, I., van der Ploeg, A.T., and Reuser, A.J.J. (2015). Enzyme therapy and immune response in relation to CRIM status: the Dutch experience in classic infantile Pompe disease. J. Inherit. Metab. Dis. *38*, 305–314. https://doi.org/10.1007/s10545-014-9707-6.

9. Koeberl, D.D., Luo, X., Sun, B., McVie-Wylie, A., Dai, J., Li, S., Banugaria, S.G., Chen, Y.T., and Bali, D.S. (2011). Enhanced efficacy of enzyme replacement therapy in Pompe disease through mannose-6-phosphate receptor expression in skeletal muscle. Mol. Genet. Metab. *103*, 107–112.

10. Prater, S.N., Patel, T.T., Buckley, A.F., Mandel, H., Vlodavski, E., Banugaria, S.G., Feeney, E.J., Raben, N., and Kishnani, P.S. (2013). Skeletal muscle pathology of infantile Pompe disease during long-term enzyme replacement therapy. Orphanet J. Rare Dis. *8*, 90. https://doi.org/10.1186/1750-1172-8-90.

11. Kazi, Z.B., Desai, A.K., Berrier, K.L., Troxler, R.B., Wang, R.Y., Abdul-Rahman, O.A., Tanpaiboon, P., Mendelsohn, N.J., Herskovitz, E., Kronn, D., et al. (2017). Sustained immune tolerance induction in enzyme replacement therapy–treated CRIM-negative patients with infantile Pompe disease. JCI Insight *2*, e94328. https://doi.org/10.1172/JCI.INSIGHT.94328.

12. Bali, D.S., Goldstein, J.L., Banugaria, S., Dai, J., Mackey, J., Rehder, C., and Kishnani, P.S. (2012). Predicting cross-reactive immunological material (CRIM) status in Pompe disease using GAA mutations: Lessons learned from 10 years of clinical laboratory testing experience. Am. J. Med. Genet. C Semin. Med. Genet. *160C*, 40–49. https://doi.org/10.1002/ajmg.c.31319.

13. Gupta, P., Shayota, B.J., Desai, A.K., Kiblawi, F., Myridakis, D., Messina, J., Tah, P., Tambini-King, L., and Kishnani, P.S. (2020). A Race Against Time—Changing the Natural History of CRIM Negative Infantile Pompe Disease. Front. Immunol. *11*, 1929. https://doi.org/10.3389/fimmu.2020.01929.

14. Diaz-Manera, J., Kishnani, P.S., Kushlaf, H., Ladha, S., Mozaffar, T., Straub, V., Toscano, A., van der Ploeg, A.T., Berger, K.I., Clemens, P.R., et al. (2021). Safety and efficacy of avalglucosidase alfa versus alglucosidase alfa in patients with late-onset Pompe disease (COMET): a phase 3, randomised, multicentre trial. Lancet Neurol. *20*, 1012–1026.

15. Schoser, B., Roberts, M., Byrne, B.J., Sitaraman, S., Jiang, H., Laforêt, P., Toscano, A., Castelli, J., Díaz-Manera, J., Goldman, M., et al. (2021). Safety and efficacy of cipaglucosidase alfa plus miglustat versus alglucosidase alfa plus placebo in late-onset Pompe disease (PROPEL): an international, randomised, double-blind, parallel-group, phase 3 trial. Lancet Neurol. *20*, 1027–1037.

16. Costa-Verdera, H., Collaud, F., Riling, C.R., Sellier, P., Nordin, J.M.L., Preston, G.M., Cagin, U., Fabregue, J., Barral, S., Moya-Nilges, M., et al. (2021). Hepatic expression of GAA results in enhanced enzyme bioavailability in mice and non-human primates. Nat. Commun. *12*, 6393. https://doi.org/10.1038/s41467-021-26744-4.

17. Eggers, M., Vannoy, C.H., Huang, J., Purushothaman, P., Brassard, J., Fonck, C., Meng, H., Prom, M.J., Lawlor, M.W., Cunningham, J., et al. (2022). Muscle-directed gene therapy corrects Pompe disease and uncovers species-specific GAA immunogenicity. EMBO Mol. Med. *14*, e13968. https://doi.org/10.15252/emmm.202113968.

18. Anzalone, A.V., Gao, X.D., Podracky, C.J., Nelson, A.T., Koblan, L.W., Raguram, A., Levy, J.M., Mercer, J.A.M., and Liu, D.R. (2022). Programmable deletion, replacement, integration and inversion of large DNA sequences with twin prime editing. Nat. Biotechnol. *40*, 731–740. https://doi.org/10.1038/s41587-021-01133-w.

19. Koblan, L.W., Doman, J.L., Wilson, C., Levy, J.M., Tay, T., Newby, G.A., Maianti, J.P., Raguram, A., and Liu, D.R. (2018). Improving cytidine and adenine base editors by expression optimization and ancestral reconstruction. Nat. Biotechnol. *36*, 843–846. https://doi.org/10.1038/nbt.4172.

20. Nelson, J.W., Randolph, P.B., Shen, S.P., Everette, K.A., Chen, P.J., Anzalone, A.V., An, M., Newby, G.A., Chen, J.C., Hsu, A., and Liu, D.R. (2022). Engineered pegRNAs improve prime editing efficiency. Nat. Biotechnol. *40*, 402–410. https://doi.org/10.1038/s41587-021-01039-7.

21. Chen, Y., Zhi, S., Liu, W., Wen, J., Hu, S., Cao, T., Sun, H., Li, Y., Huang, L., Liu, Y., et al. (2020). Development of highly efficient dual-AAV split adenosine base editor for *in vivo* gene therapy. Small Methods *4*, 2000309. https://doi.org/10.1002/smtd.202000309.

22. Davis, J.R., Wang, X., Witte, I.P., Huang, T.P., Levy, J.M., Raguram, A., Banskota, S., Seidah, N.G., Musunuru, K., and Liu, D.R. (2022). Efficient *in vivo* base editing via single adeno-associated viruses with size-optimized genomes encoding compact adenine base editors. Nat. Biomed. Eng. *6*, 1272–1283. https://doi.org/10.1038/s41551-022-00911-4.

23. Zhi, S., Chen, Y., Wu, G., Wen, J., Wu, J., Liu, Q., Li, Y., Kang, R., Hu, S., Wang, J., et al. (2022). Dual-AAV delivering split prime editor system for *in vivo* genome editing. Mol. Ther. *30*, 283–294. https://doi.org/10.1016/j.ymthe.2021.07.011.

24. Skopenkova, V.V., Egorova, T.V., and Bardina, M.V. (2021). Muscle-Specific Promoters for Gene Therapy. Acta Naturae *13*, 47–58. https://doi.org/10.32607/actanaturae.11063.

25. Monteys, A.M., Hundley, A.A., Ranum, P.T., Tecedor, L., Muehlmatt, A., Lim, E., Lukashev, D., Sivasankaran, R., and Davidson, B.L. (2021). Regulated control of gene therapies by drug-induced splicing. Nature *596*, 291–295. https://doi.org/10.1038/s41586-021-03770-2.

26. Gaudelli, N.M., Komor, A.C., Rees, H.A., Packer, M.S., Badran, A.H., Bryson, D.I., and Liu, D.R. (2017). Programmable base editing of A•T to G•C in genomic DNA without DNA cleavage. Nature *551*, 464–471. https://doi.org/10.1038/nature24644.

27. Bose, S.K., White, B.M., Kashyap, M.V., Dave, A., De Bie, F.R., Li, H., Singh, K., Menon, P., Wang, T., Teerdhala, S., et al. (2021). In utero adenine base editing corrects multi-organ pathology in a lethal lysosomal storage disease. Nat. Commun. *12*, 4291. https://doi.org/10.1038/s41467-021-24443-8.

28. Newby, G.A., Yen, J.S., Woodard, K.J., Mayuranathan, T., Lazzarotto, C.R., Li, Y., Sheppard-Tillman, H., Porter, S.N., Yao, Y., Mayberry, K., et al. (2021). Base editing of haematopoietic stem cells rescues sickle cell disease in mice. Nature *595*, 295–302. https://doi.org/10.1038/s41586-021-03609-w.

29. Anzalone, A.V., Randolph, P.B., Davis, J.R., Sousa, A.A., Koblan, L.W., Levy, J.M., Chen, P.J., Wilson, C., Newby, G.A., Raguram, A., and Liu, D.R. (2019). Search-and-replace genome editing without double-strand breaks or donor DNA. Nature *576*, 149–157. https://doi.org/10.1038/s41586-019-1711-4.

30. Kurt, I.C., Zhou, R., Iyer, S., Garcia, S.P., Miller, B.R., Langner, L.M., Grünewald, J., and Joung, J.K. (2021). CRISPR C-to-G base editors for inducing targeted DNA transversions in human cells. Nat. Biotechnol. *39*, 41–46. https://doi.org/10.1038/s41587-020-0609-x.

31. Tong, H., Wang, X., Liu, Y., Liu, N., Li, Y., Luo, J., Ma, Q., Wu, D., Li, J., Xu, C., and Yang, H. (2023). Programmable A-to-Y base editing by fusing an adenine base editor with an N-methylpurine DNA glycosylase. Nat. Biotechnol. *41*, 1080–1084. https://doi.org/10.1038/s41587-022-01595-6.

32. Kluesner, M.G., Nedveck, D.A., Lahr, W.S., Garbe, J.R., Abrahante, J.E., Webber, B.R., and Moriarity, B.S. (2018). EditR: A Method to Quantify Base Editing from Sanger Sequencing. CRISPR J. *1*, 239–250. https://doi.org/10.1089/crispr.2018.0014.

33. Conant, D., Hsiau, T., Rossi, N., Oki, J., Maures, T., Waite, K., Yang, J., Joshi, S., Kelso, R., Holden, K., et al. (2022). Inference of CRISPR Edits from Sanger Trace Data. CRISPR J. *5*, 123–130.

34. Clement, K., Rees, H., Canver, M.C., Gehrke, J.M., Farouni, R., Hsu, J.Y., Cole, M.A., Liu, D.R., Joung, J.K., Bauer, D.E., and Pinello, L. (2019). CRISPResso2 provides accurate and rapid genome editing sequence analysis. Nat. Biotechnol. *37*, 224–226. https://doi.org/10.1038/s41587-019-0032-3.

35. Singh, R.R. (2020). Next-Generation Sequencing in High-Sensitive Detection of Mutations in Tumors: Challenges, Advances, and Applications (Elsevier B.V.). https://doi.org/10.1016/j.jmoldx.2020.04.213.

36. Bae, S., Park, J., and Kim, J.S. (2014). Cas-OFFinder: A fast and versatile algorithm that searches for potential off-target sites of Cas9 RNA-guided endonucleases. Bioinformatics *30*, 1473–1475. https://doi.org/10.1093/bioinformatics/btu048.

37. Hsu, P.D., Scott, D.A., Weinstein, J.A., Ran, F.A., Konermann, S., Agarwala, V., Li, Y., Fine, E.J., Wu, X., Shalem, O., et al. (2013). DNA targeting specificity of RNA-guided Cas9 nucleases. Nat. Biotechnol. *31*, 827–832. https://doi.org/10.1038/nbt.2647.

38. Tsai, S.Q., Nguyen, N.T., Malagon-Lopez, J., Topkar, V.V., Aryee, M.J., and Joung, J.K. (2017). CIRCLE-seq: A highly sensitive *in vitro* screen for genome-wide CRISPR-Cas9 nuclease off-targets. Nat. Methods *14*, 607–614. https://doi.org/10.1038/nmeth.4278.

39. Scalzitti, N., Kress, A., Orhand, R., Weber, T., Moulinier, L., Jeannin-Girardon, A., Collet, P., Poch, O., and Thompson, J.D. (2021). Spliceator: multi-species splice site prediction using convolutional neural networks. BMC Bioinf. *22*, 561. https://doi.org/10.1186/s12859-021-04471-3.

40. Will, C.L., and Lührmann, R. (2011). Spliceosome structure and function. Cold Spring Harbor Perspect. Biol. *3*, 1–2. https://doi.org/10.1101/cshperspect.a003707.

41. Carapuça, E., Azzoni, A.R., Prazeres, D.M.F., Monteiro, G.A., and Mergulhão, F.J.M. (2007). Time-course determination of plasmid content in eukaryotic and prokaryotic cells using Real-Time PCR. Mol. Biotechnol. *37*, 120–126. https://doi.org/10.1007/s12033-007-0007-3.

42. Freeze, H.H., and Kranz, C. (2010). Endoglycosidase and glycoamidase release of N-linked glycans. Curr. Protoc. Mol. Biol. *Chapter 17*. Unit 17.13A. https://doi.org/10.1002/0471142727.mb1713as89.

43. Maley, F., Trimble, R.B., Tarentino, A.L., and Plummer, T.H., Jr. (1989). Characterization of glycoproteins and their associated oligosaccharides through the use of endoglycosidases. Anal. Biochem. *180*, 195–204.

44. Fukuda, T., Ahearn, M., Roberts, A., Mattaliano, R.J., Zaal, K., Ralston, E., Plotz, P.H., and Raben, N. (2006). Autophagy and Mistargeting of Therapeutic Enzyme in Skeletal Muscle in Pompe Disease. Mol. Ther. *14*, 831–839. https://doi.org/10.1016/j.ymthe.2006.08.009.

45. Raben, N., Fukuda, T., Gilbert, A.L., de Jong, D., Thurberg, B.L., Mattaliano, R.J., Meikle, P., Hopwood, J.J., Nagashima, K., Nagaraju, K., and Plotz, P.H. (2005). Replacing acid α-glucosidase in Pompe disease: Recombinant and transgenic enzymes are equipotent, but neither completely clears glycogen from type II muscle fibers. Mol. Ther. *11*, 48–56. https://doi.org/10.1016/j.ymthe.2004.09.017.

46. Nilsson, M.I., Crozier, M., Di Carlo, A., Xhuti, D., Manta, K., Roik, L.J., Bujak, A.L., Nederveen, J.P., Tarnopolsky, M.G., Hettinga, B., et al. (2022). Nutritional co-therapy with 1,3-butanediol and multi-ingredient antioxidants enhances autophagic clearance in Pompe disease. Mol. Genet. Metab. *137*, 228–240. https://doi.org/10.1016/j.ymgme.2022.06.001.

47. Levy, J.M., Yeh, W.-H., Pendse, N., Davis, J.R., Hennessey, E., Butcher, R., Koblan, L.W., Comander, J., Liu, Q., and Liu, D.R. (2020). Cytosine and adenine base editing of the brain, liver, retina, heart and skeletal muscle of mice via adeno-associated viruses. Nat. Biomed. Eng. *4*, 97–110. https://doi.org/10.1038/s41551-019-0501-5.

48. Weinmann, J., Weis, S., Sippel, J., Tulalamba, W., Remes, A., El Andari, J., Herrmann, A.K., Pham, Q.H., Borowski, C., Hille, S., et al. (2020). Identification of a myotropic AAV by massively parallel *in vivo* evaluation of barcoded capsid variants. Nat. Commun. *11*, 5432. https://doi.org/10.1038/s41467-020-19230-w.

49. Tabebordbar, M., Lagerborg, K.A., Stanton, A., King, E.M., Ye, S., Tellez, L., Krunnfusz, A., Tavakoli, S., Widrick, J.J., Messemer, K.A., et al. (2021). Directed evolution of a family of AAV capsid variants enabling potent muscle-directed gene delivery across species. Cell *184*, 4919–4938.e22. https://doi.org/10.1016/j.cell.2021.08.028.

50. Kleinstiver, B.P., Prew, M.S., Tsai, S.Q., Topkar, V.V., Nguyen, N.T., Zheng, Z., Gonzales, A.P.W., Li, Z., Peterson, R.T., Yeh, J.R.J., et al. (2015). Engineered CRISPR-Cas9 nucleases with altered PAM specificities. Nature *523*, 481–485. https://doi.org/10.1038/nature14592.

51. Harb, J.F., Christensen, C.L., Kan, S.-H., Rha, A.K., Andrade-Heckman, P., Pollard, L., Steet, R., Huang, J.Y., and Wang, R.Y. (2023). Base editing corrects the common Salla disease SLC17A5 c.115C>T variant. Mol. Ther. Nucleic Acids *34*, 102022. https://doi.org/10.1016/j.omtn.2023.08.024.

52. Schneider, C.A., Rasband, W.S., and Eliceiri, K.W. (2012). NIH Image to ImageJ: 25 years of image analysis. Nat. Methods *9*, 671–675.